PAB3D Simulations for the CAWAPI F- 16XL

Alaa Elmiligui[1]
Analytical Services & Materials, Inc. Hampton, VA 23666

K.S. Abdol-Hamid [2]
NASA Langley Research Center, Hampton VA 23681

and
Steven J. Massey[3]
Eagle Aeronautics, Hampton, VA 23666

Numerical simulations of the flow around F-16XL are performed as a contribution to the Cranked Arrow Wing Aerodynamic Project International (CAWAPI) using the PAB3D CFD code. Two turbulence models are used in the calculations: a standard k-ε model, and the Shih-Zhu-Lumley (SZL) algebraic stress model. Seven flight conditions are simulated for the flow around the F-16XL where the free stream Mach number varies from 0.242 to 0.97. The range of angles of attack varies from 0° to 20°. Computational results, surface static pressure, boundary layer velocity profiles, and skin friction are presented and compared with flight data. Numerical results are generally in good agreement with flight data, considering that only one grid resolution is utilized for the different flight conditions simulated in this study. The ASM results are closer to the flight data than the k-ε model results. The ASM predicted a stronger primary vortex, however, the origin of the vortex and footprint is approximately the same as in the k-ε predictions.

Nomenclature

ASM	=	algebraic stress model
BL	=	butt line on airplane, positive on right wing
CAWAP	=	Cranked Arrow Wing Aerodynamics Project
CAWAPI	=	Cranked Arrow Wing Aerodynamics Project International
CFD	=	Computational Fluid Dynamics
Cp	=	static-pressure coefficient
cf	=	local skin friction coefficient
FC	=	Flight Condition
FS	=	Fuselage Station on airplane
F-16XL	=	an extensively modified version of the F-16A aircraft which is longer and has a cranked arrow wing instead of a trapezoidal wing with leading-edge strake
HSRP	=	High Speed Research Program
HSCT	=	High Speed Civil Transport
ITAR	=	Iinternational Traffic in Arms Regulations
LaRC	=	Langley Research Center
LE	=	leading edge

---

[1] Senior Research Scientist, AIAA Member.
[2] Aerospace Engineer, Configuration Aerodynamics Branch, AIAA Associate Fellow.
[3] Senior Research Scientist, AIAA Member.

M_∞	=	Free-stream Mach number
NASA	=	National Aeronautics and Space Administration
NATO	=	North Atlantic Treaty Organization
RANS	=	Reynolds Averaged Navier-Stokes
Rn	=	Reynolds number
SZL	=	Shih-Zhu-Lumley
T	=	absolute temperature, °R
USM3D	=	Unstructured grid flow solver developed at NASA Langley and component of TetRUSS
V/VRE	=	ratio of velocity magnitude in boundary layer to that at the Rake Extreme total-pressure tube
VL	=	Virtual Laboratory
WL	=	waterline on airplane
u_τ	=	friction velocity
x/c	=	fractional distance along the local chord, positive aft
y	=	normal distance above the surface at a rake location
y^+	=	dimensionless normal distance from the wall based on the law of the wall, $u_\tau y/\nu$
$\propto$	=	angle of attack
β	=	angle of side-slip
ν	=	kinematic molecular viscosity
$2y/b_1$	=	fractional distance along the wing local semi-span, positive toward the right wing tip

I. Introduction

The CAWAPI utilized the F-16XL aircraft as part of a basic research project planned in support of the High Speed Research Program (HSRP). Review of the project and how it evolved over the years is given by Lamar & Obara[1]. Flight, wind-tunnel and computational studies were conducted, and various data sets were generated, analyzed, and compared[2,3]. The Virtual Laboratory (VL) environment and common data standards to store the data were established. The Virtual Laboratory was housed in an electronically secure area; details about VL have been documented in References 4 and 5.

CAWAPI objectives were to validate new methodologies and to evaluate a number of predictive methods against available flight test data at high Reynolds numbers, and to check the Technology Readiness Level of Computational Fluid Dynamics (CFD) codes for a military aircraft. Military requirements result in a need for a better understanding of the aircraft characteristics before full-scale production. For this purpose, new and existing CFD codes have to be validated, and their Technology Readiness Level checked and/or increased. To meet these objectives, several numerical studies[7-16] have been conducted to compute and compare predicted flow around the F-16XL with flight data. CAWAPI members embraced the idea of engaging in a cooperative venture. The benefits from validated CFD codes are enhanced analysis of system performance prior to flight, as well as tools to aid in the understanding of unexpected flight behavior.

In the present study, simulations are conducted using PAB3D CFD code[17], which is a structured, multiblock, parallel, implicit, finite-volume solver of the three-dimensional Unsteady Reynolds Averaged Navier-Stokes (URANS) equations; advanced turbulence models are available in the code. PAB3D is widely used for internal and external flow applications by NASA and by the US aerospace industry. PAB3D has several built-in timesaving routines including grid sequencing and customized computer memory requirements that permit the user to quickly obtain a converged solution. There are several state-of-the-art two-equation and algebraic Reynolds stress turbulence models implemented in the PAB3D code. PAB3D has been well-tested and documented for the simulation of aero-propulsive and aerodynamic flows involving separation, mixing, and other complicated phenomena[18]. PAB3D is ported to a number of platforms and offers a combination of good performance and low memory requirements. In addition to its advanced pre-processor, which can handle complex geometries through multi-block general patching, PAB3D has a runtime module capable of calculating aerodynamic performance on the fly as well as a post processor[19] used for follow-on data analysis.

This present paper describes and analyzes a series of CFD test cases performed as a contribution to the CAWAPI project. The organization of this paper is as follows: (1) the description of PAB3D features, (2) the governing equations and the turbulence models used in this study, (3) a brief description of the F-16XL geometry and the computational grid, (4) presentation of the numerical results along with discussion and comparison to flight data[2], and (5) the concluding remarks.

II. Computational Fluid Dynamics Simulation

In this study, PAB3D is used in conjunction with two-equation k-ε turbulence closure and nonlinear algebraic Reynolds stress models to simulate flow around F-16XL. PAB3D solves the simplified Reynolds-averaged Navier-Stokes equations in conservative form. Viscous models include coupled and uncoupled simplified Navier-Stokes and thin layer Navier-Stokes options. Roe's upwind scheme is used to evaluate the explicit part of the governing equations, and van Leer's scheme is used for the implicit part. Diffusion terms are centrally differenced, inviscid terms are upwind differenced, and two finite volume flux-splitting schemes are used to construct the convective flux terms. PAB3D is third-order upwind biased accurate in space, and second-order accurate in time.

III. Governing Equations

The governing equations solved in this study are the time-averaged Reynolds Averaged Navier-Stokes (RANS). The perfect gas law is chosen to represent the air properties.

$$\frac{\partial \rho}{\partial t} + \frac{\partial \rho u_i}{\partial x_i} = 0$$

$$\frac{\partial \rho u_i}{\partial t} + \frac{\partial (\rho u_i u_j + p\delta_{ij})}{\partial x_j} = \frac{\partial (\tau_{ij} - \rho \overline{u_i u_j})}{\partial x_j}$$

$$\frac{\partial \rho e_0}{\partial t} + \frac{\partial (\rho e_0 u_i + p u_i)}{\partial x_i} = \frac{\partial (\tau_{ij} u_j - \rho \overline{u_i u_j} u_j)}{\partial x_i} - \frac{\partial (q_i + C_P \rho \overline{u_i \theta})}{\partial x_i} + \frac{\partial}{\partial x_i}\left[\left(\propto_l + \frac{\propto_t}{\overline{\sigma}_k}\right)\frac{\partial k}{\partial x_i}\right]$$

(1)

IV. RANS Closure

Two turbulence models are used in the current study to model turbulence: a standard k-ε model, and Shih-Zhu-Lumley (SZL) algebraic stress model[20].

A. Two Equation k-ε model

To close the RANS equations, the two-equation (k-ε) turbulence model is given by:

$$\frac{\partial \rho k}{\partial t} + \frac{\partial \rho u_j k}{\partial x_j} = -\rho \overline{u_j u_i}\frac{\partial u_i}{\partial x_j} + \frac{\partial}{\partial x_j}\left[\rho\left(v_l + \frac{c_\propto k^2}{\overline{\sigma}_k \varepsilon}\right)\frac{\partial k}{\partial x_j}\right] - \rho\varepsilon$$

$$\frac{\partial \rho \varepsilon}{\partial t} + \frac{\partial \rho u_j \varepsilon}{\partial x_j} = -C_{\varepsilon 1}\rho \overline{u_j u_i}\frac{\partial u_i}{\partial x_j}\frac{\varepsilon}{k} + \frac{\partial}{\partial x_j}\left[\rho\left(v_l + \frac{c_\propto k^2}{\overline{\sigma}_\varepsilon \varepsilon}\right)\frac{\partial \varepsilon}{\partial x_j}\right] - f_2\tilde{C}_{\varepsilon 2}\rho\frac{\varepsilon}{k}\left[\varepsilon - v_l\left(\frac{\partial \sqrt{k}}{\partial x_j}\right)^2\right]$$

(2)

$$C_\propto = 0.09, C_{\varepsilon 1} = 1.44$$

$$\overline{\sigma}_k = \sigma_k = 1.4, \overline{\sigma}_\varepsilon = \sigma_\varepsilon = 1 \text{ and } \overline{C_{\varepsilon 2}} = C_{\varepsilon 2} = 1.92$$

The turbulent stress components are formulated as:

$$-\rho \overline{u_i u_j} = \tau_{ij}^L + \tau_{ij}^{NL}$$

(3)

The linear contribution to the stress is

$$\tau_{ij}^L = -2\rho v_t S_{ij} + \frac{2}{3}\delta_{ij}\rho k$$

(4)

where, $S_{ij} = \dfrac{1}{2}\left[\dfrac{\partial u_i}{\partial x_j} + \dfrac{\partial u_j}{\partial x_i}\right] - \dfrac{1}{3}\delta_{ij}\dfrac{\partial u_k}{\partial x_k}$ (5)

For the purpose of this paper, RANS turbulent viscosity is defined as

$$v_t^{RANS} = f_\propto C_\propto \frac{k^2}{\varepsilon}$$ (6)

In the case of a linear RANS simulation

$$v_t = v_t^{RANS} \quad and \quad C_\propto = 0.09$$

B. Algebraic Reynolds Stress

$C_\propto$ is 0.09 for the linear model and is a function of vorticity and strain tensors for the nonlinear models. In the SZL nonlinear model[20], the turbulent stresses are given by:

$$-\overline{u_i u_j} = 2v_t S_{ij} - \frac{2}{3}\delta_{ij}k - 2\beta\frac{k^3}{\varepsilon^2}(W_{ik}S_{kj} - S_{ik}W_{kj})$$ (7)

Algebraic stress models give inherently better results than the linear stress model because of the explicit modeling of effects such as relaxation and the specific inclusion of nonlinear anisotropic effects from the mean flow strain and vortices. A compilation of the parameters used in the turbulence models can be found in Reference 21.

V. Computational Domain and Boundary Conditions

The F-16XL airplane is a single-place fighter-type prototype aircraft developed by the General Dynamics Corporation, Fort Worth Division (now Lockheed Martin Aeronautics Company – Fort Worth). The design of the cranked-arrow wing was a cooperative effort of the NASA Langley Research Center and the General Dynamics Corporation. Figure 1 shows a picture of the F-16XL airplane in flight. The technical specifications for the airplane are given in Table 1.

Table 1: Airplane Specifications, *from Lamar & Obara[1]*

Feature	Value
Wing Span	32.4 ft.
Height	17.606 ft.
Length	54.155 ft.
Reference Chord	24.7 ft.
Theoretical Root Chord	41.75 ft.
Wing Area	646.37 ft^2
Reference Wing Area	600 ft^2
Reference Aspect Ratio	1.75
Typical Takeoff Weight	35,000 lbs.
Engine; Max Thrust	Pratt & Whitney F100-PW-200; 23,830 lbs.

Description of the F-16XL geometry and computational grids used in CAWAPI are given in Reference 6. The computational grid used in this study consisted of 14.7 million cells and 200 blocks, and is shown in Figure 2. The original grid generated by Boelens[6] et al had 214 blocks; a number of blocks were merged to enhance efficiency

during parallel computations. The angles of side-slip β for FC7, FC19, FC 25, FC 46, & FC 70 were all less than 1, and hence one half of the aircraft was simulated with plane of symmetry boundary condition imposed at the symmetry plane. A no-slip boundary condition was applied to all solid surfaces, and a Riemann invariant characteristic type boundary condition was applied to far field boundaries. Constant total values were specified for the nozzle inlet, and constant pressure boundary condition was specified at the nozzle exit. For FC 50 and FC 51 the side-slip angle, β, is approximately 5° and the flow around the full aircraft was simulated. The computational grid consisted of 400 blocks and 29.5 million cells and was generated by mirroring the modified grid around the symmetry plane. On average, the grid first cell height was approximately y^+<1.2. The far field boundaries extend six root chords to far field.

VI. Computational Results

The flow field was computed using PAB3D[17] for seven flight conditions. Two turbulence models were used to model turbulence: the standard k-ε model, and the SZL algebraic stress model (ASM)[20]. Table 2 and 3 list the seven flight conditions modeled in this study.

Table 2: Seven Flight Conditions, from Lamar & Obara[1]

Flight Condition	Actual Mach No.	Actual α	Actual β	Actual Reynolds No.
FC7	0.304	11.89	-0.133	44.4E+06
FC19	0.36	11.85	+0.612	46.8E+06
FC46	0.527	10.4	+0.684	46.9E+06
FC70	0.97	4.37	+0.310	88.77E+06
FC25	0.242	19.84	0.725	32.22E+06
FC50	0.434	13.56	+5.31	39.41E+06
FC51	0.441	12.89	-4.58	38.95E+06

Table 3: Associated Engine Parameters* for these Flight Conditions, from Lamar & Obara[1]

Flight Condition	Free Stream Altitude, ft.	Free Stream Mach	Inlet Duct Exit Static Temp., degs. R	Inlet Duct Exit Static Press., psia	Inlet Duct Exit Velocity, ft/sec.	Inlet Duct Exit Mach	Mixing Plane Total Temp., degs. R	Mixing Plane Total Press., psia
FC7	5000	0.304	498	11	379.6	0.347	1050	23
FC19	10000	0.36	485.8	10.2	345.8	0.32	1050	21.5
FC46	24000	0.527	443.6	5.85	404.3	0.39	1045	14.8
FC70	22300	0.97	519	10.65	464.7	0.416	1200	30
FC25	10000	0.242	470.1	8.72	474.8	0.447	1209	26.3
FC50	24000	0.434	440	5.16	483.3	0.47	1154	16.95
FC51	24000	0.441	431.8	5.19	468.6	0.46	1146	16.74

*The numbers in this table do not represent any particular engine.

Grid sequencing was used to accelerate convergence by solving 1/4 then 1/2 of the grid in each of the three computational directions. To insure convergence, all the simulations performed in this study ran 5,000 iterations at each of the coarse grid levels and 10,000 iterations on the fine grid level. Figure 3 shows convergence history of FC 7 using both turbulence models. All simulations ran on a 2.8 GHz PC cluster, at the Configuration Aerodynamics Branch of NASA Langley Research Center. For FC7, FC19, FC 25, FC 46, & FC 70, only half of the aircraft was modeled and 56 processors were used while the full aircraft was modeled for FC 50 & FC 51, and 113 processors

were used. A typical run for the fully converged solution at the fine grid level on a 14.7 million cell grid and 200 blocks required 51 wall clock hours on 56 PC nodes, with the solver running in parallel at a speed on the order of 1.12 ∝sec/cell for k-ε calculations and 1.24 ∝sec/cell for ASM calculations. Surface pressure distributions for FC 46, boundary layer profiles for FC 7, and skin friction are presented. This is followed by comparison between PAB3D, the unstructured grid solver USM3D[16], and flight data for FC 50. Finally, surface pressure distribution for FC 70 is presented.

Figure 4(a) to (n) shows comparison between computed results and flight data for FC 46. There is a general overall agreement between computed results and PAB3D predictions. On the suction peak at BL 55, k-ε results under-predicted the primary vortex effect. The ASM over predicted flight data at BL 70 through BL 105 and under predicted flight data at BL 153.5. Figure 5 shows that the vortex predicted with the ASM is stronger than that predicted with the k-ε model and also shows that the k-ε model failed to accurately predict the secondary vortex. Figure 4(i) through 4(o) also shows that the k-ε model failed to predict the secondary vortex. Figure 6 shows the grid distribution on the upper surface of the wing and the vortex core location for both the k-ε and ASM models. The vortex origin and footprint are approximately the same for both sets of computations. The reason for the slight discrepancy between predicted values and flight data is due to the coarse nature of the grid on the upper surface, as shown in Figure 6. To better resolve the flow field on the upper surface of the wing, more points are needed in both the chord wise and in the span wise directions. Areas where a finer grid can render a better prediction are pointed out on Figure 6. The vortex core location superimposed on Cp contours is shown Figure 7 for both the ASM and k-ε models. Although the ASM predicted a stronger vortex, as shown in Figure 7, the vortex origin and footprint is approximately the same.

The computed and flight[1] boundary layer profiles for FC 7 are shown in Figure 8. The horizontal axis in Figure 8 is the normalized velocity magnitude which is defined as ratio of the velocity magnitude in boundary layer to that at the last rake position. The results for rake 3, FS 302.17, and BL -52.93 are shown in Figure 8(a), where the flow is nearly in the stream wise direction. Both turbulence models show qualitative good agreement with the flight data, with the k-ε model giving a slightly better prediction than the ASM. However, Figure 8(b) shows that the ASM gives better quantitative agreement with flight data than the k-ε model. Figure 8(c) shows results for rake 5, where the k-ε model gives better comparison with flight data than the ASM, which over predicts the flight data. For rake 7, the k-ε model underestimates the flight data while the ASM over predicts it. Figure 8(c) and Figure 8(d) show that the flight data and numerical predictions are not asymptotic at the rake extreme, which is indicative that the edge of the boundary layer has not been captured. Contours of the upper surface Cp for FC 7 are shown in Figure 9. Both models predict Cp better inboard and along the leading edge. The ASM predicted a stronger vortex compared to the k-ε predictions.

Figure 10 shows a comparison between the computed PAB3D, USM3D[16], and measured local skin friction at FS 330 for FC19. Computed and flight data show good qualitative agreement. Both sets of data capture the two suction peaks, which are an indication of a primary and secondary vortex being present above the wing surface. The USM3D k-ε solution over-predicts the peak of the primary vortex by 7.5% while the PAB3D k-ε model under predicts flight data by 9.4%. The PAB3D ASM model matches the flight data better than the USM3D k-ε and the PAB3D k-ε model, even though that high suction peak of the ASM model under predicts flight data by 15%. Figure 11 shows the computed upper surface Cp contours for FC19. Similar to FC 7, the ASM predicted a stronger vortex compared to the k-ε model predictions. The k-ε model failed to accurately predict the secondary vortex.

For FC 50 and FC 51, the flow around the full aircraft was simulated. For FC 50, the side-slip angle, β, is +5.31° while for FC 51, the side-slip angle, β, is -4.58°. Figure 12 and 13 show Cp contours using ASM for FC 50 and FC 51 respectively. Figure 14 shows comparison between computed PAB3D, USM3D[16], and flight data for FC 50. All three models compare well with flight data. The USM3D k-ε model captures the suction peak better than PAB3D on the inner wing for BL 55. PAB3D ASM indicated the presence of a secondary vortex for BL 70, BL 80, & BL 95, while the k-ε model for both PAB3D and USM3D failed to predict the secondary vortex. The suction rise and peak were also higher for the ASM case. All models failed to accurately capture compression on the upper surface. As pointed out in the previous section, more points are needed on the upper surface to accurately capture the compression on the upper surface. All three models predicted the lower surface well. A detailed comparison for the effect of turbulence modeling for F-16Xl USM3D predictions is given in reference[16].

Figure 15(a) through (n) shows comparison between PAB3D computed results and flight data for the transonic flight condition (FC 70). Figure 15(o) shows comparison between PAB3D ASM and k-ε calculations of upper surface Cp contours for FC 70. Figure 15 shows that calculated results deviate from the flight data, similar behavior was reported by CAWAPI researchers[7-16], for FC 70. Figure 15 indicates that the effect of the turbulence model is negligible for this flight condition.

VII. Concluding Remarks

Numerical simulations of the flow around F-16XL were performed as a contribution to the CAWAPI using the PAB3D CFD code. The flow field was computed for seven flight conditions. Two turbulence models were used in the calculations: a standard k-ε model, and Shih-Zhu-Lumley (SZL) algebraic stress model[20]. Surface static pressure, boundary layer velocity profiles, and skin friction were presented and compared to flight data. There is a general good agreement between computed results and flight data. The ASM results are closer to the flight data than the k-ε model results. The ASM predicted a stronger primary vortex, however, the origin of the vortex and the footprint is approximately the same as in the k-ε predictions. The reason for the slight discrepancy between predicted values and flight data is due to the coarse nature of the grid on the upper surface. Comparison with USM3D results, for FC 50, shows good agreement. Results emphasized the conclusion that the algebraic stress models give inherently better results than the linear stress model because of the explicit modeling of effects such as relaxation, and the specific inclusion of nonlinear anisotropic effects from the mean flow strain and vortices. Future work would involve generating a new grid with a y+ <1, and increasing the number of grids in the boundary layer and concentrating grid points on the upper surface in regions where high flow gradients occur.

Acknowledgments

References

[1] Lamar, John E., Obara, Clifford J.; "Review of Cranked-Arrow Wing Aerodynamics Project: Its International Aeronautical Community Role. AIAA Paper 2007-0487, Presented at 45th AIAA Aerospace Presented at 45th AIAA Aerospace Sciences Meeting and Exhibit, Reno NV, January 8-11, 2007.

[2] Lamar, John E., Obara, Clifford J.; Fisher, Bruce D.; and Fisher, David F.: Flight, Wind-Tunnel, and Computational Fluid Dynamics Comparison for Cranked Arrow Wing (F-16XL-1) at Subsonic and Transonic Speeds. NASA/TP-2001-210629, February 2001.

[3] Wendy B. Lessard: ``Subsonic Analysis of 0.04-Scale F-16XL Models Using an Unstructured Euler Code,'' NASA TP 3597, October 1996

[4] Lamar, John E.; Conin, Catherine K.; and Scott, Laura E.: A Review of Steps Taken to Create an International Virtual Laboratory at NASA Langley for Aerodynamic Prediction and Comparison. Prog Aerospace ci, Vol. 40, p.163-172, 2004.

[5] Lamar, John E.; Cronin, Catherine K.; and Scott, Laura E.: Virtual Laboratory Enabling Collaborative Research in Applied Vehicle Technologies. In AVT-123 Symposium on "Flow Induced Unsteady Loads and the Impact on Military Applications", Keynote 2, Budapest, Hungary, April 25-29, 2005.

[6] Boelens, O.J.; Goertz, S.; Morton, S.A.; Fritz, W.; and Lamar, J.E.: Description of the F-16XL Geometry and Computational Grids Used in CAWAPI. AIAA Paper 2007-0488, 45th AIAA Aerospace Presented at 45th AIAA Aerospace Sciences Meeting and Exhibit, Reno NV, January 8-11, 2007.

[7] Boelens, O.J.; Spekreijse, S.P.; Sytsma, H.A.; and de Cock, K.M.J.: Comparison of measured and simulated flow features for the full-scale F-16XL aircraft. AIAA Paper 2007-0489, 45th AIAA Aerospace Presented at 45th AIAA Aerospace Sciences Meeting and Exhibit, Reno NV, January 8-11, 2007.

[8] Badcock, K.J.: Evaluation of Results from a Reynolds Averaged Multiblock Code Against F-16XL Flight Data. AIAA Paper 2007-0490, 45th AIAA Aerospace Sciences Meeting and Exhibit, Reno NV, January 8-11, 2007.

[9] Fritz, W.: Hybrid Grid RANS Solutions for the CAWAPI F-16XL. AIAA Paper 2007-0492, 45th AIAA Aerospace Sciences Meeting and Exhibit, Reno NV, January 8-11, 2007.

[10] Morton. S.A.; McDaniels, D.R.; and Cummings, R.M.: F-16XL Unsteady Simulations for the CAWAPI Facet of RTO Task Group AVT-113. AIAA Paper 2007-0493, 45th AIAA Aerospace Sciences Meeting and Exhibit, Reno NV, January 8-11, 2007.

[11] Goertz, S. and Jirasek, A.: Unstructured Steady/Unsteady Solutions with Edge for CAWAPI F-16XL at KTH/FOI. AIAA Paper 2007-0678, 45th AIAA Aerospace Sciences Meeting and Exhibit, Reno NV, January 8-11, 2007.

[12] Michal, T.; Oser, M.; Mani, M.; and Ross, F.: BCFD Unstructured-Grid Predictions on the F-16XL (CAWAPI) Aircraft. AIAA Paper 2007-0679, 45th AIAA Aerospace Sciences Meeting and Exhibit, Reno NV, January 8-11, 2007.

[13] Michal, T.; Oser, M.; Mani, M.; and Ross, F.: BCFD Unstructured-Grid Predictions on the F-16XL (CAWAPI) Aircraft. AIAA Paper 2007-0679, Presented at 45th AIAA Aerospace Presented at 45th AIAA Aerospace Sciences Meeting and Exhibit, Reno NV, January 8-11, 2007.

[14]   Davis, M.B.; Reed, C.; and Yagle, P.: Hybrid Grid Solutions on the (CAWAPI) F-16XL Using Falcon v4. AIAA Paper 2007-0680, 45th AIAA Aerospace Sciences Meeting and Exhibit, Reno NV, January 8-11, 2007.

[15]   Karman, S.; Mitchell, B.; and Sawyer, S.: Unstructured Grid Solutions of CAWAPI F-16XL by UT SimCenter. AIAA Paper 2007-0681, 45th AIAA Aerospace Sciences Meeting and Exhibit, Reno NV, January 8-11, 2007.

[16]   Lamar, J.E. and Abdol-Hamid, K.S.: USM3D Unstructured Grid Solutions for CAWAPI at NASA LaRC. AIAA Paper 2007-0682, 45th AIAA Aerospace Sciences Meeting and Exhibit, Reno NV, January 8-11, 2007.

[17]   PAB3D Code Manual Originally developed by the Propulsion Aerodynamics Branch, now under cooperative program between the Configuration Aerodynamics Branch, NASA Langley Research Center and Analytical Services & Materials, Inc. Hampton, VA. See http://www.asm-usa.com/software/pab3d.html

[18]   Abdol-Hamid, K., Pao, S. P., Hunter, C., Deere, K. A., Massey, S. J., and Elmiligui, A. " PAB3D: Its History in the Use of Turbulence Models in the Simulation of Jet and Nozzle Flows", AIAA-2006-489, 44th AIAA Aerospace Sciences Meeting and Exhibit, Reno, Nevada, Jan. 9-12, 2006.

[19]   Massey, S. J., POST Code Manual, See http://www.asm-usa.com/post/

[20]   Shih, T.H., Zhu, J., and Lumley, J.L. "A New Reynolds Stress Algebraic Equation Model". NASA TM-106644, August 1994.

[21]   Elmiligui, A., Abdol-Hamid, K., and Hunter, C. "Numerical Investigation Flow in an Over-Expanded Nozzle with Porous Surfaces", AIAA Paper 2005-4159, Tucson, Arizona, 2005

Figure 1. Missiles, tufts, modified flow-visualization paint scheme, and video targets on airplane at Dryden Flight Research Center (NASA Photo EC96-43508-2)[1].
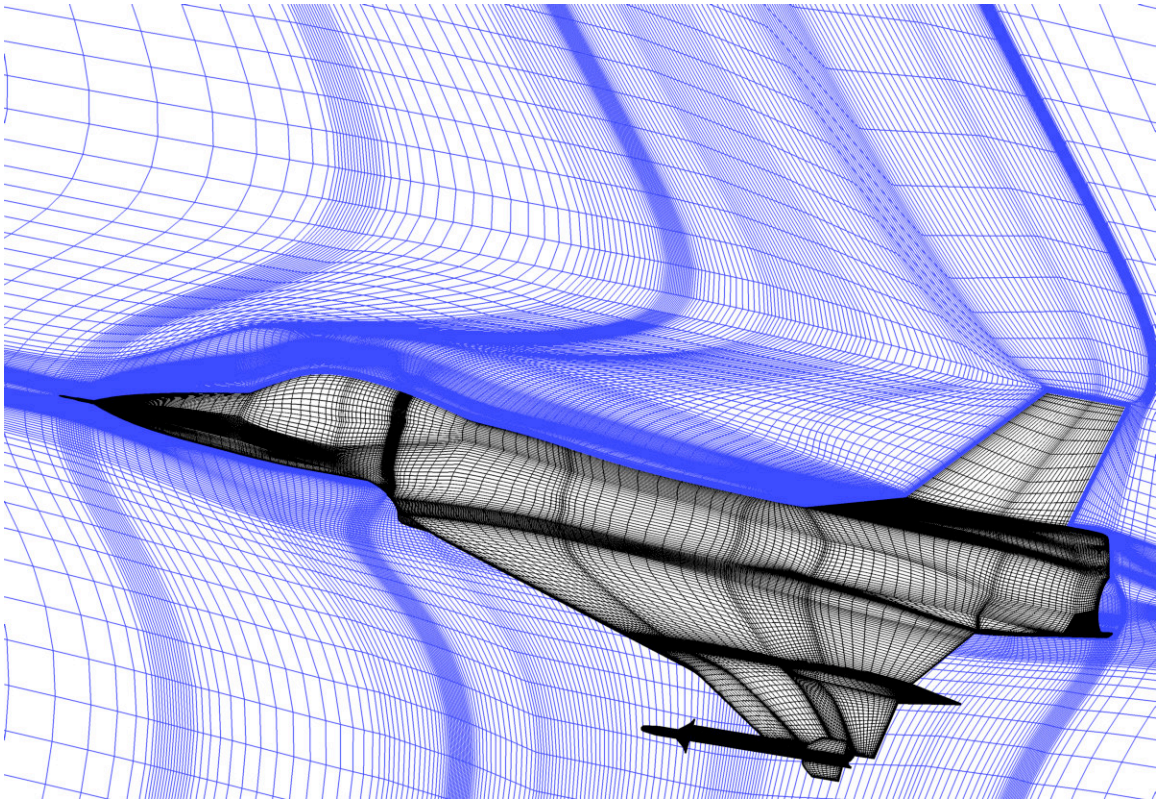
Figure 2. Computational grid on wing-fuselage.
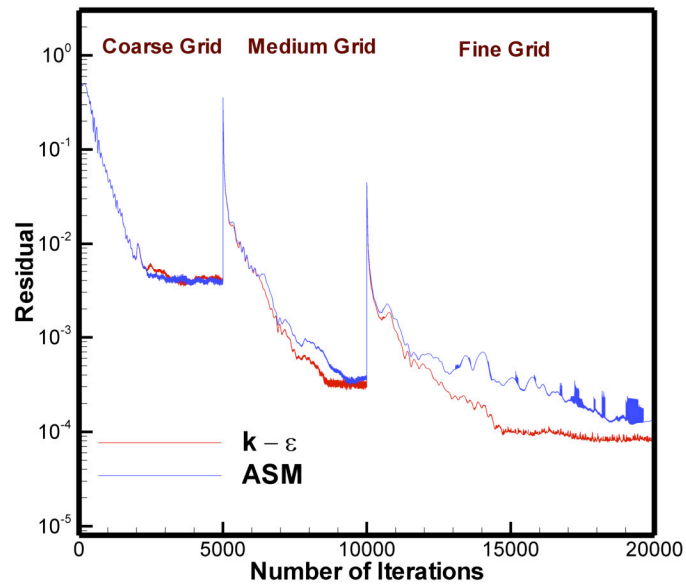
Figure 3. Convergence history for FC 7 M=0.304, $\alpha = 11.89$, $R_n= 44.4 \ X10^{6}$.

(a) BL 55

(b) BL 70

(c) BL 80

(d) BL 95

(e) BL 105

(f) BL 153.5
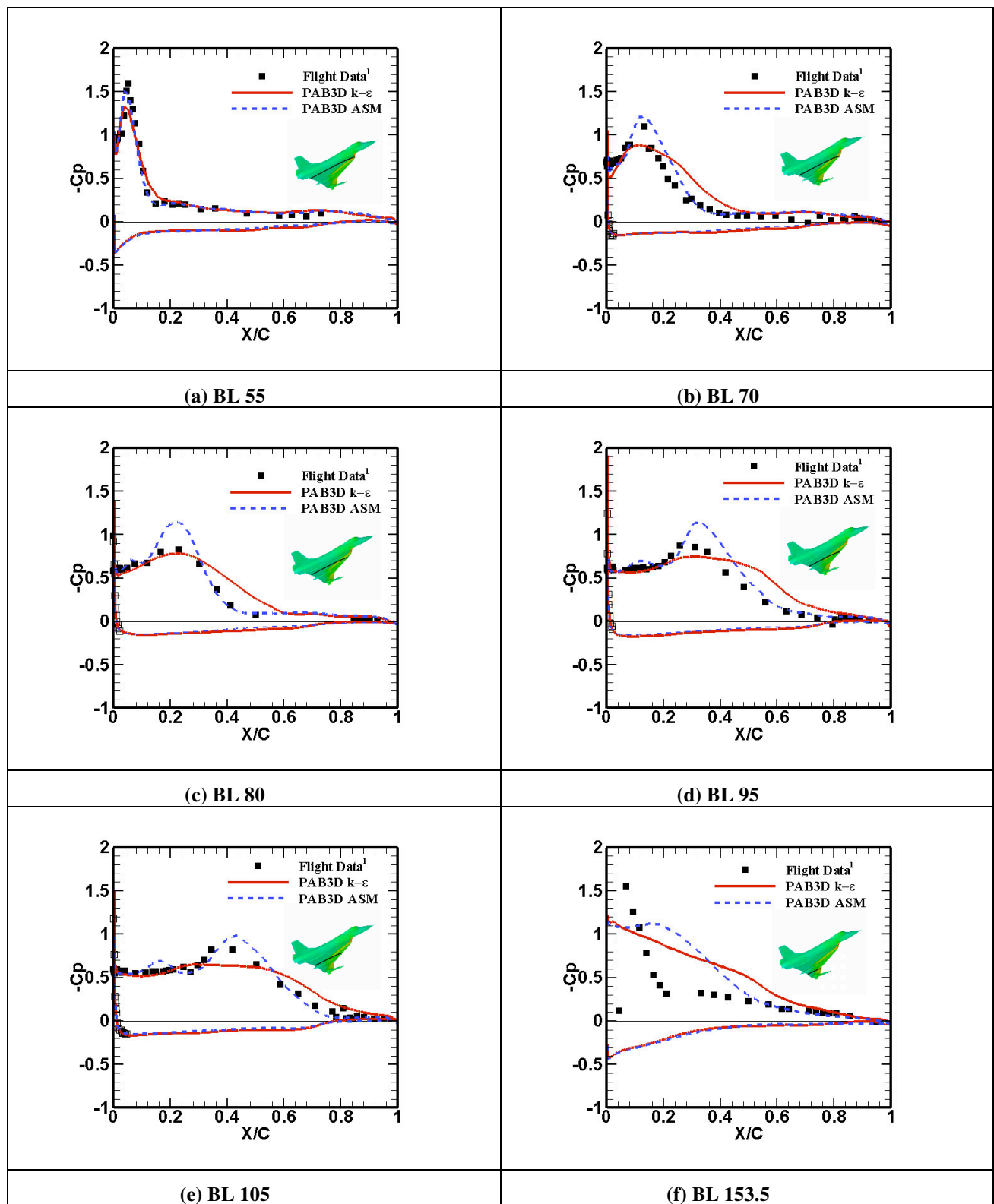
Figure 4. Computed and measured flight C_p at FC 46 (M=0.527, α = 10.4 , R_n= 46.9 X 10^6).

(g) BL 184.5

(h) FS 185

(i) FS 300

(j) FS 337.5

(k) FS 375

(l) FS 407.5
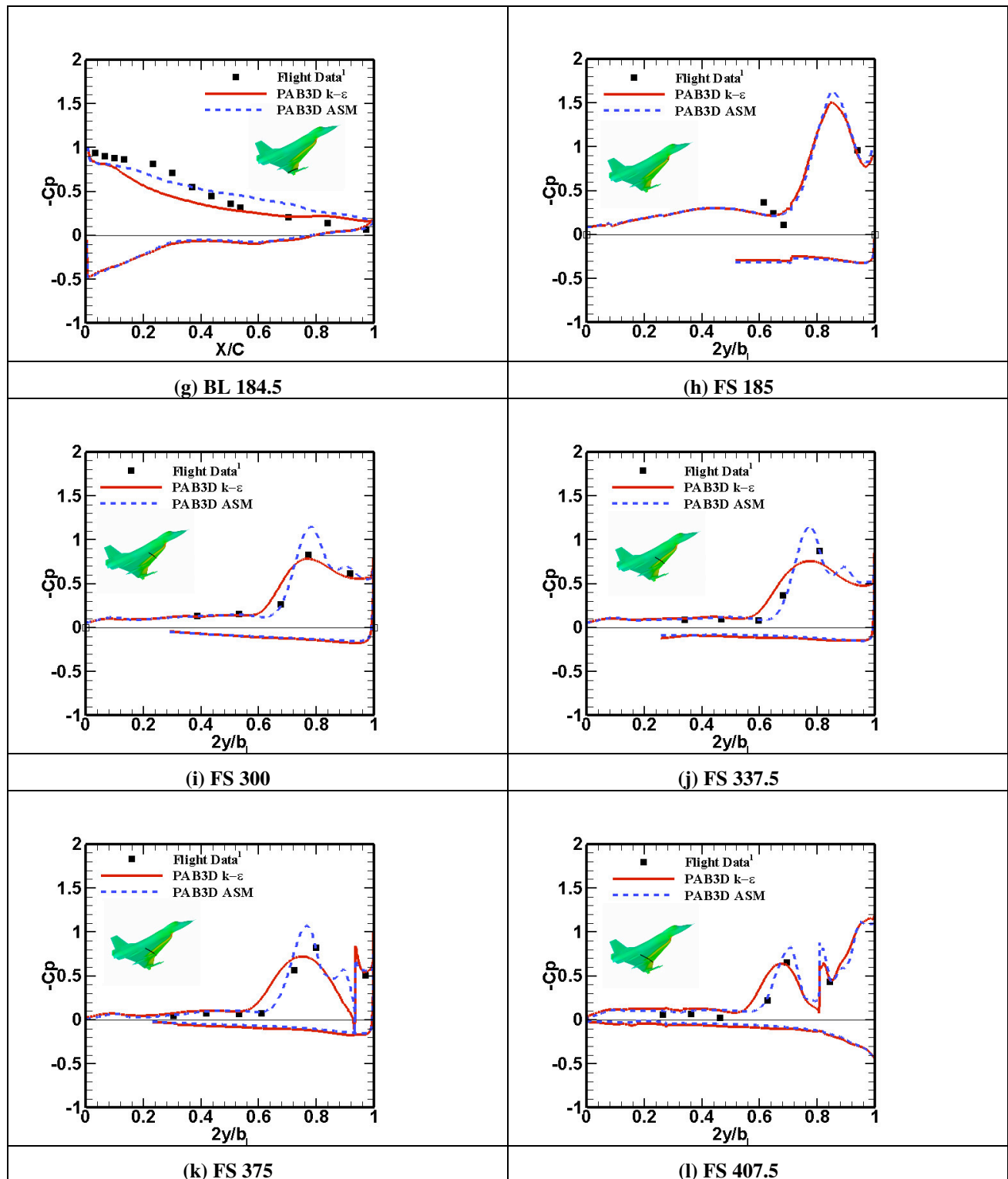
Figure 4. Continued
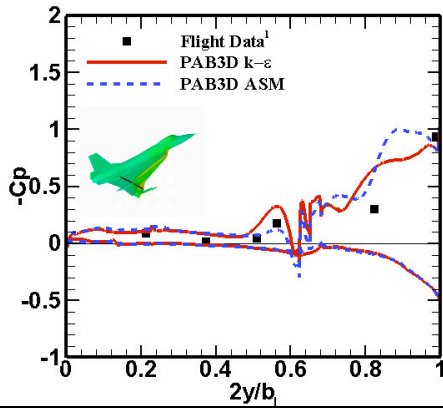
(m) FS 450
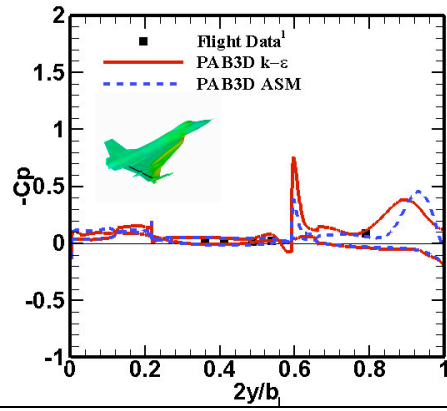
(n) FS 492.5
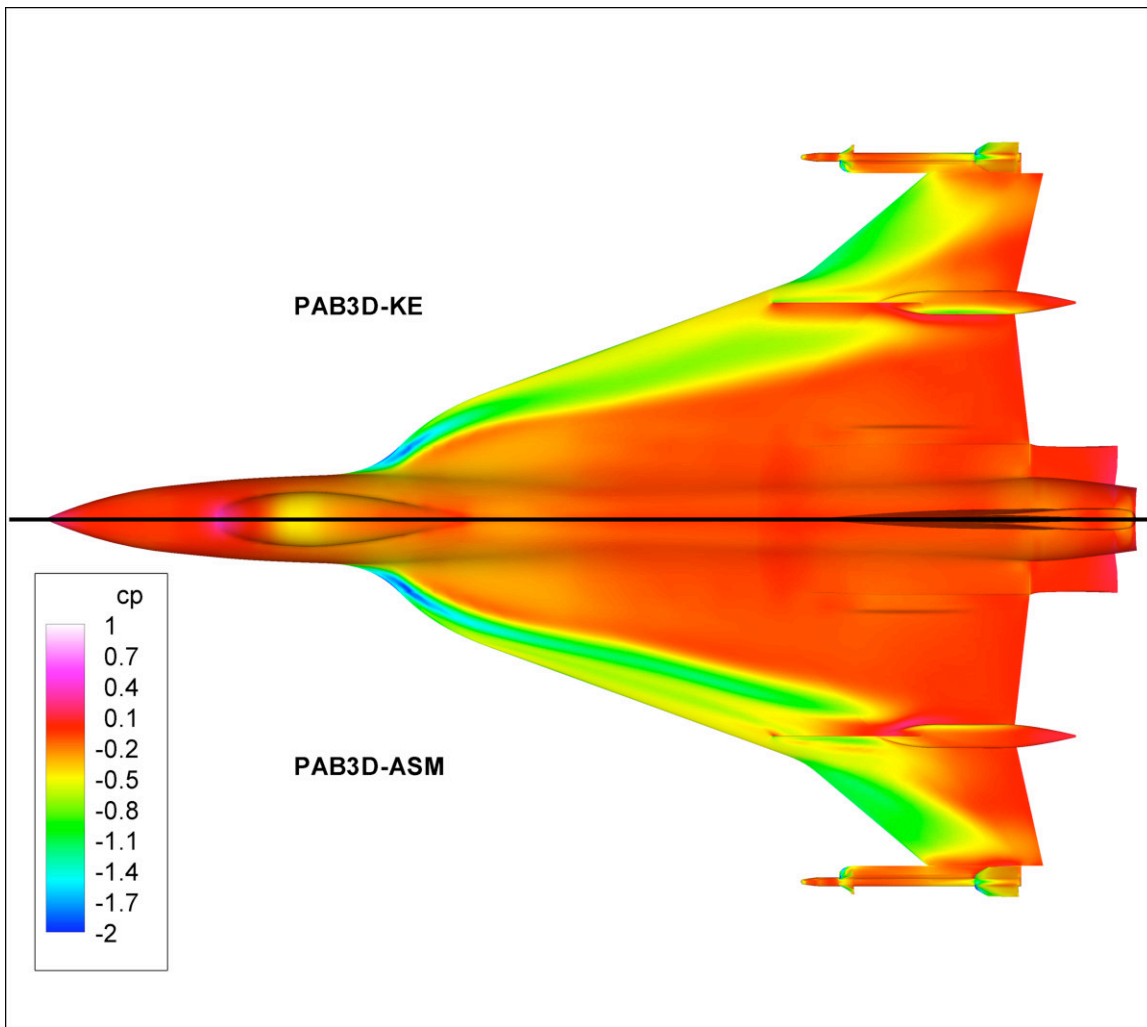
(o) Upper Surface C$_p$

Figure 4. Concluded.
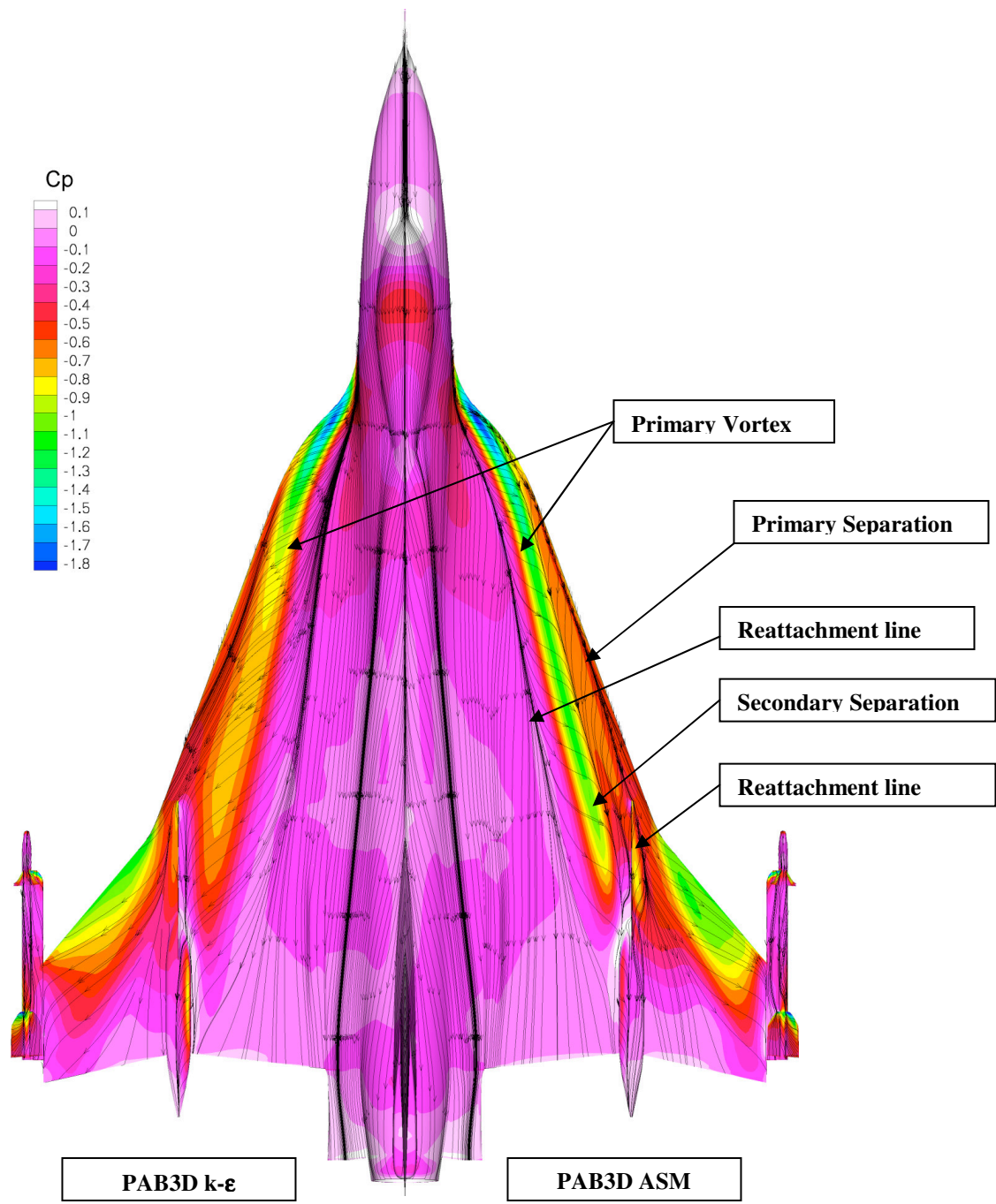
Figure 5. Upper surface pressure distribution with streamlines FC 46 (M=0.527, α = 10.4 , R_n= 46.9 X 10^6).

More grid is needed in these areas
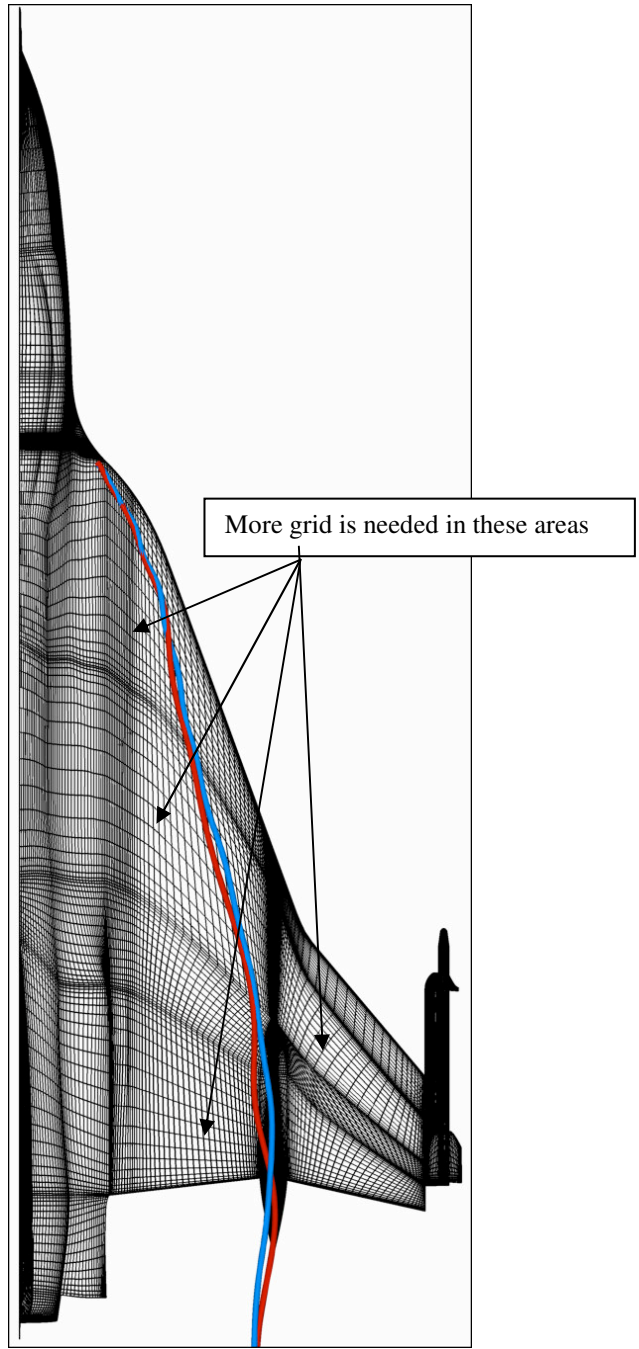
━━━━ **Vortex Core location for PAB3D k-ε**

━━━━ **Vortex Core location for PAB3D ASM**

Figure 6. Surface with vortex core location for FC 46 (M=0.527, α = 10.4 , R_n= 46.9 X 10^6).
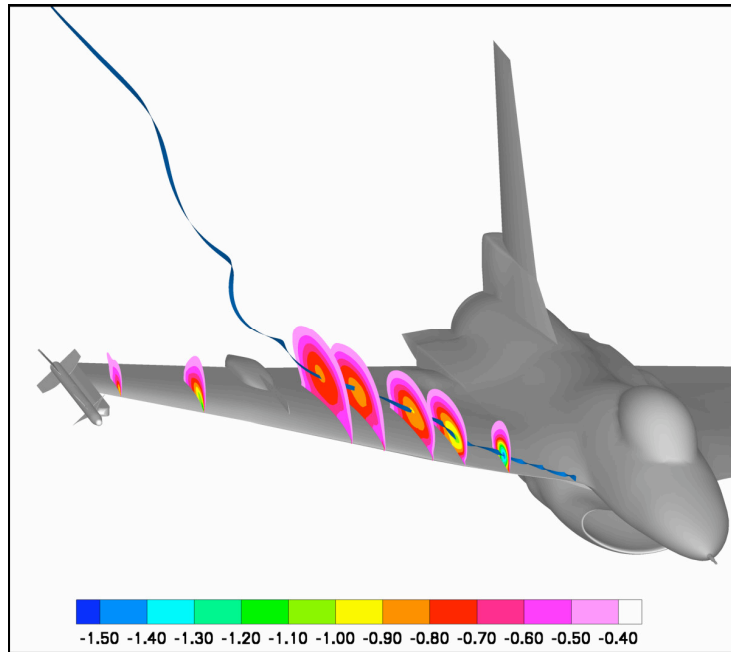
(a) PAB3D k-ε
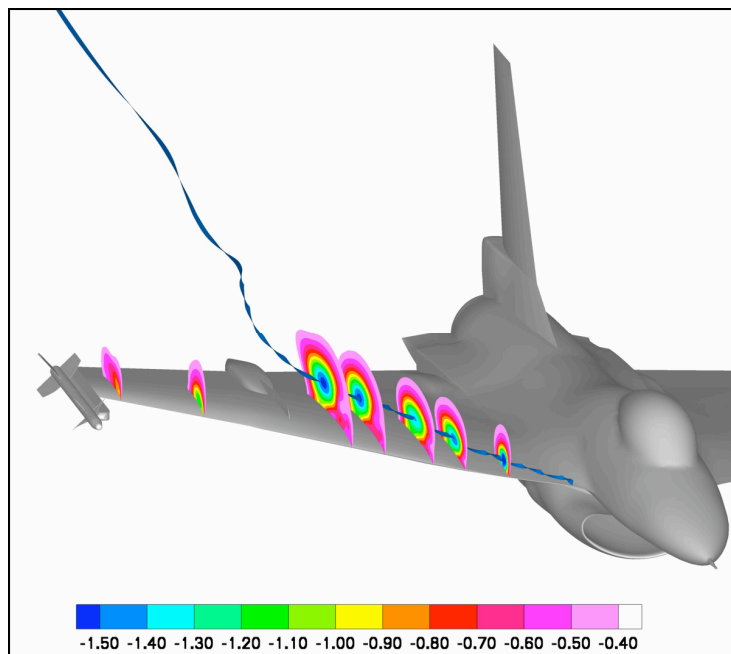
(b) PAB3D ASM

Figure 7. Cp contours with vortex core representation FC 46 (M=0.527, α = 10.4 , R_n= 46.9 X 10^6).
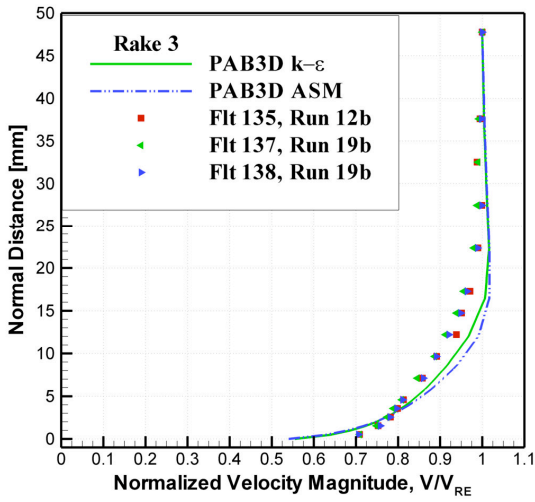
(a) Rake 3; FS .302.17, BL -52.93.
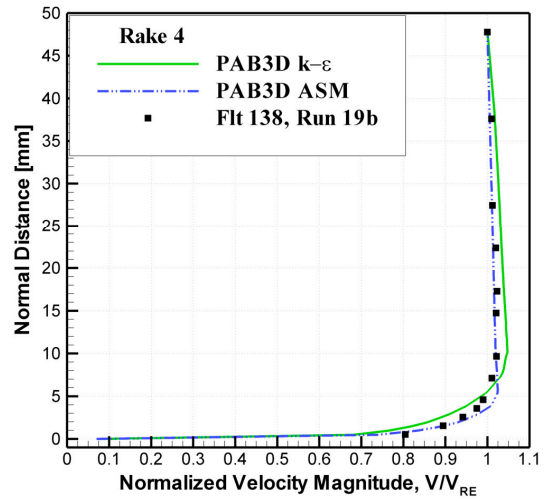
(b) Rake 4; FS 293.45, BL -76.22.
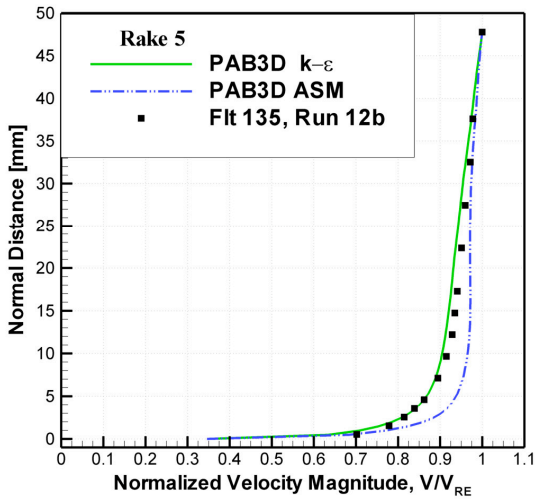
(c) Rake 5; FS 295.52, BL -94.33.
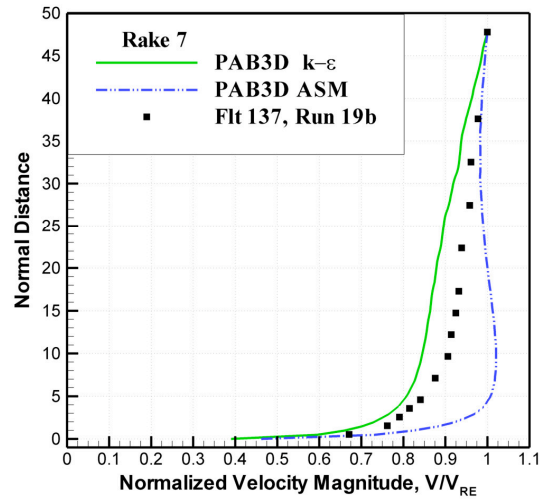
(d) Rake 7; FS 294.59, BL -96.06.

Figure 8. Velocity Profiles for Boundary Layer Rakes on F-16XL for FC 7 M_∞=0.304, α = 11.89 , R_n= 44.4 X10^6.
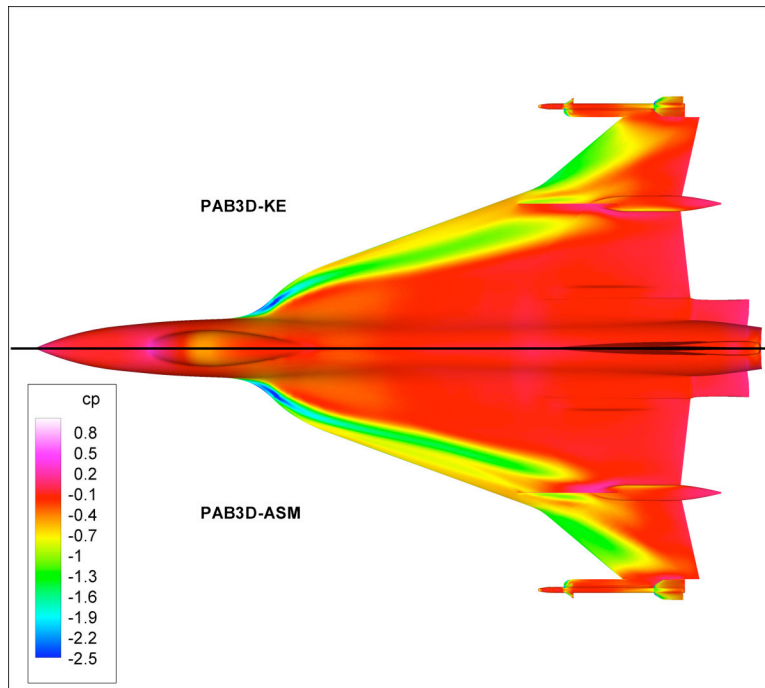
Figure 9. Upper surface pressure distribution for FC 7 M$_\infty$=0.304, α = 11.89 , R$_n$= 44.4 X10^6.
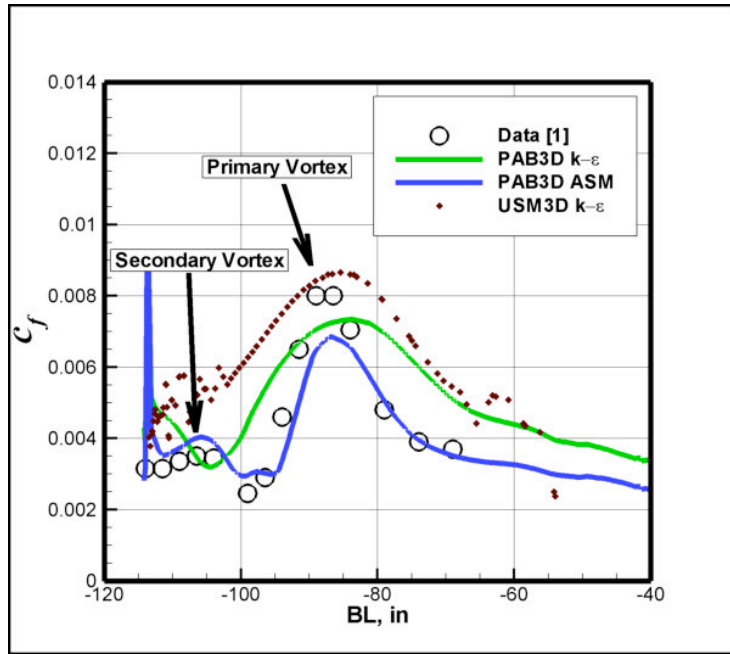
Figure 10. Skin Friction on F-16Xl Aircraft at FS 330 for FC 19 M_∞=0.36, α = 11.85 , R_n= 46.8 X10^6 .
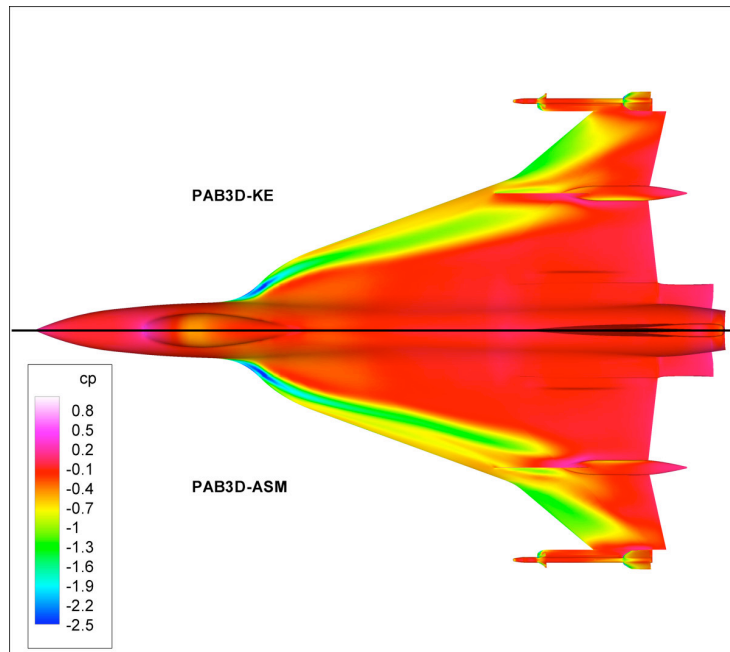
Figure 11. Upper surface pressure distribution for FC 19 M_∞=0.36, α = 11.85 , R_n= 46.8 X10^6.

Wind [Aircraft at 5.31 ° of sideslip]

PAB3D-KE

cp

0.8
0.5
0.2
-0.1
-0.4
-0.7
-1
-1.3
-1.6
-1.9
-2.2
-2.5
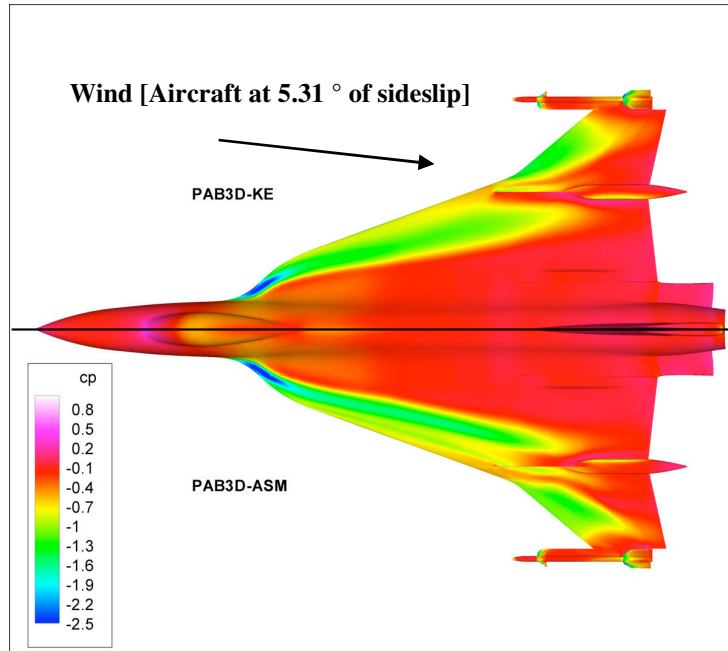
PAB3D-ASM

Figure 12. Upper surface pressure distribution for FC 50 (M=0.434, α = 13.56 , β = +5.31, R_n=39.4 X 10^6).

PAB3D-KE

cp

0.8
0.5
0.2
-0.1
-0.4
-0.7
-1
-1.3
-1.6
-1.9
-2.2
-2.5

PAB3D-ASM

Wind [Aircraft at -4.58 °of sideslip]
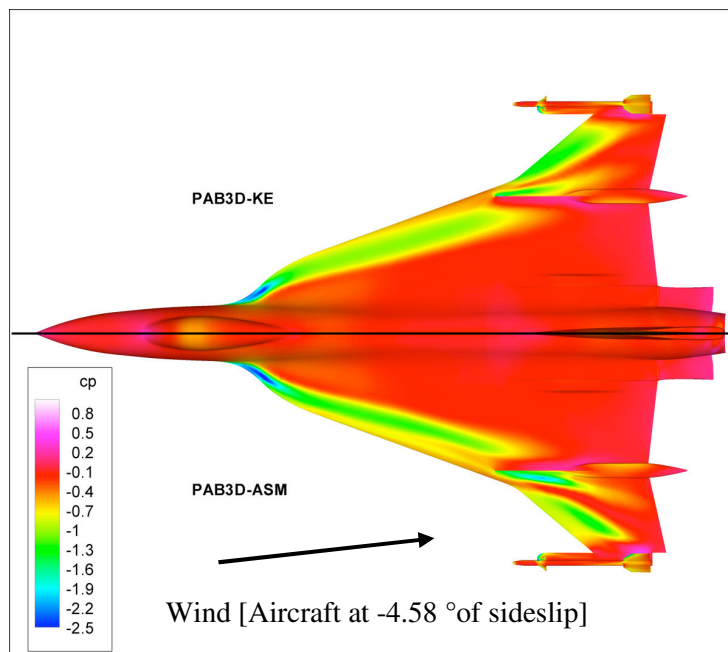
Figure 13. Upper surface pressure distribution for FC 51 (M=0.441, α = 12.89 , β = -4.58, R_n= 38.9 X 10^6).

(a) BL 55

(b) BL 70

(c) BL 80

(d) BL 95

(e) BL 105

(f) BL 153.5
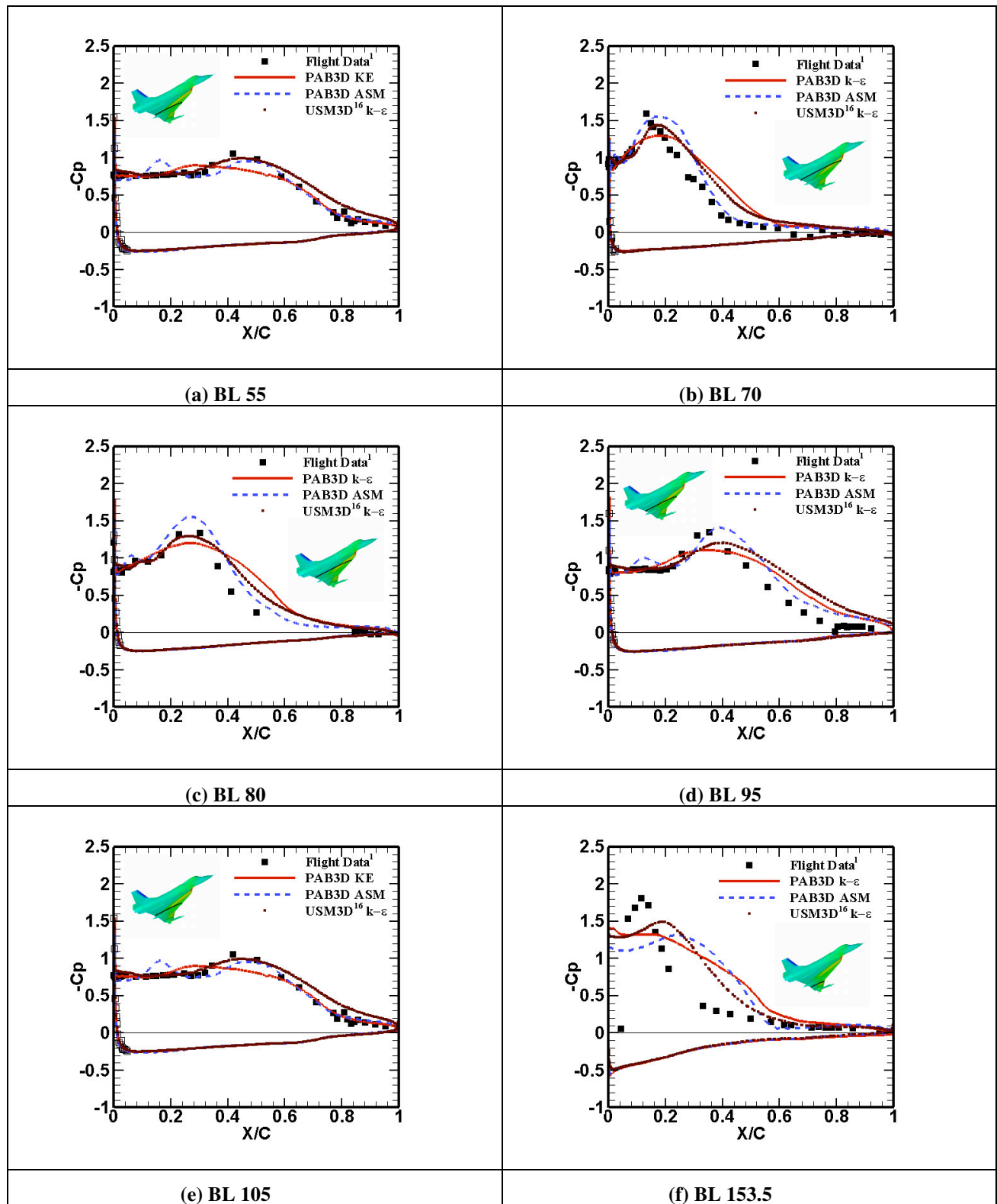
Figure 14. Comparison between PAB3D and USM3D C_p for FC 50 (M=0.434, α = 13.56 , β = +5.31, R_n=39.4 X 10^6).

(g) BL 184.5

(h) FS 185

(i) FS 300
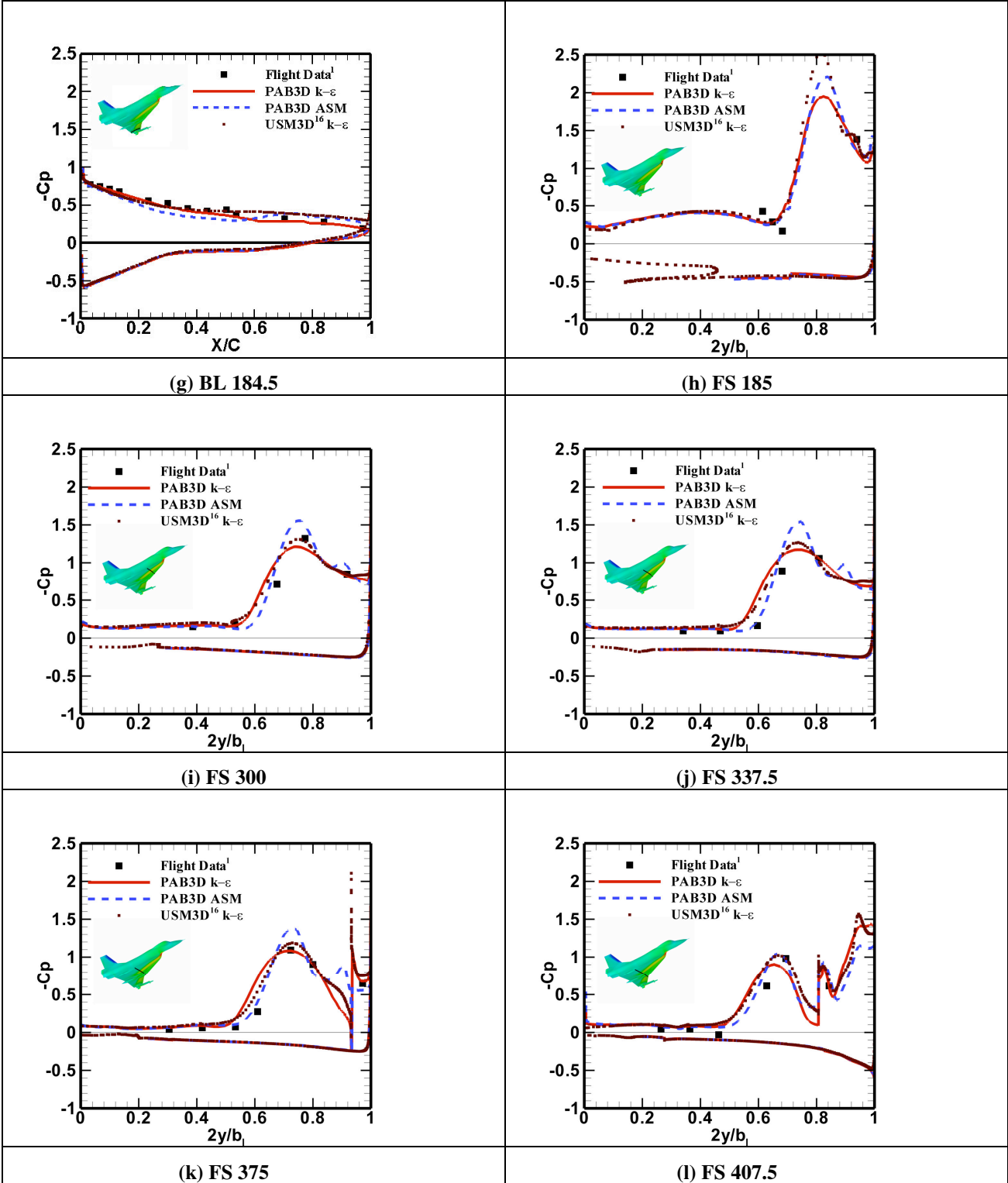
(j) FS 337.5
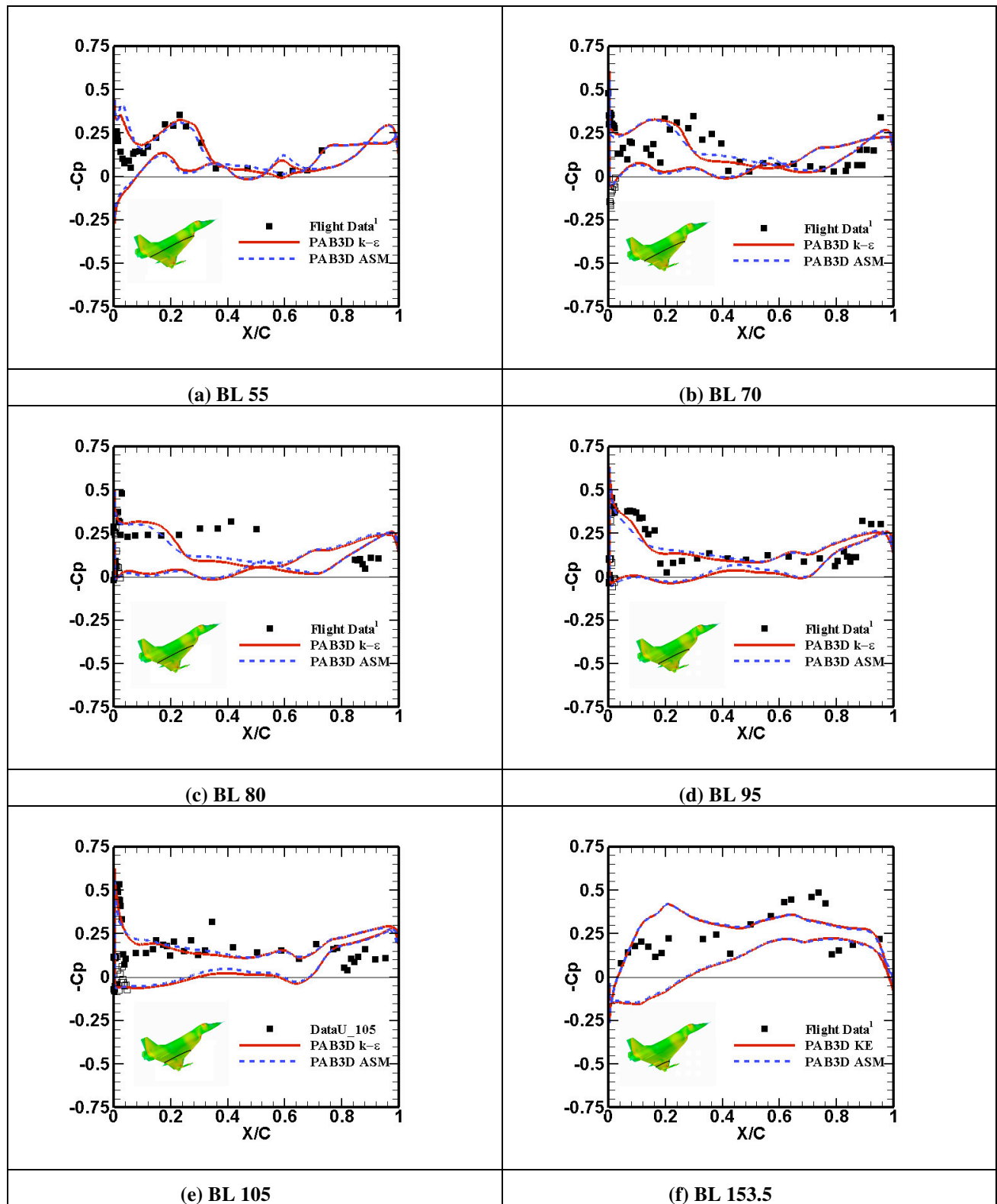
(k) FS 375

(l) FS 407.5

Figure 14 Concluded.

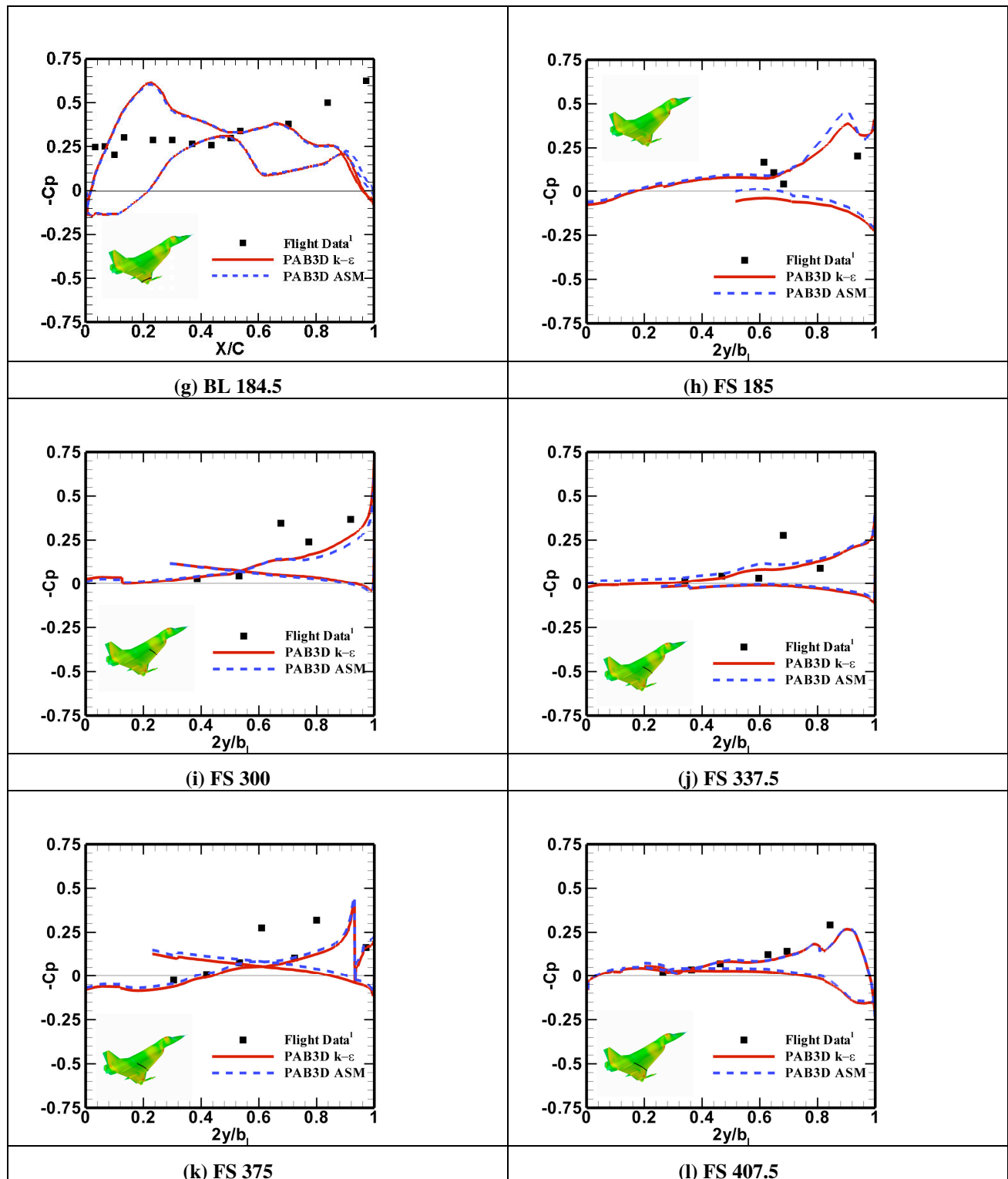Figure 15. Computed and measured flight C_p at FC 70 (M=0.97, α = 4.37 , R_n= 88.77 X 10^6).

(g) BL 184.5

(h) FS 185

(i) FS 300

(j) FS 337.5
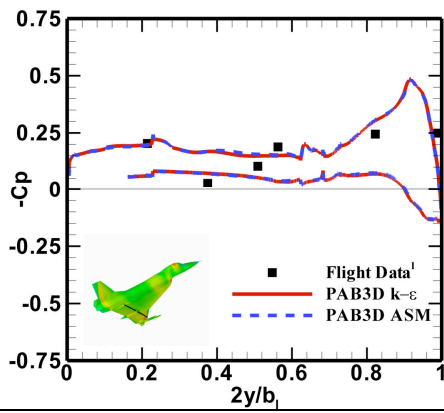
(k) FS 375

(l) FS 407.5

Figure 15 Continued
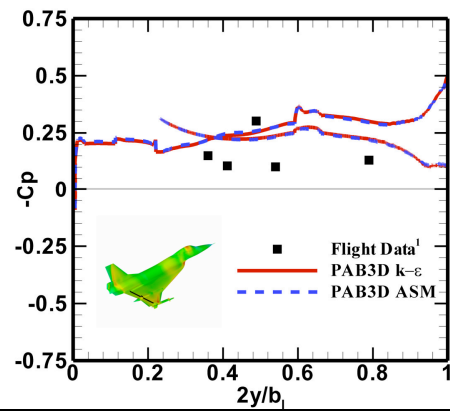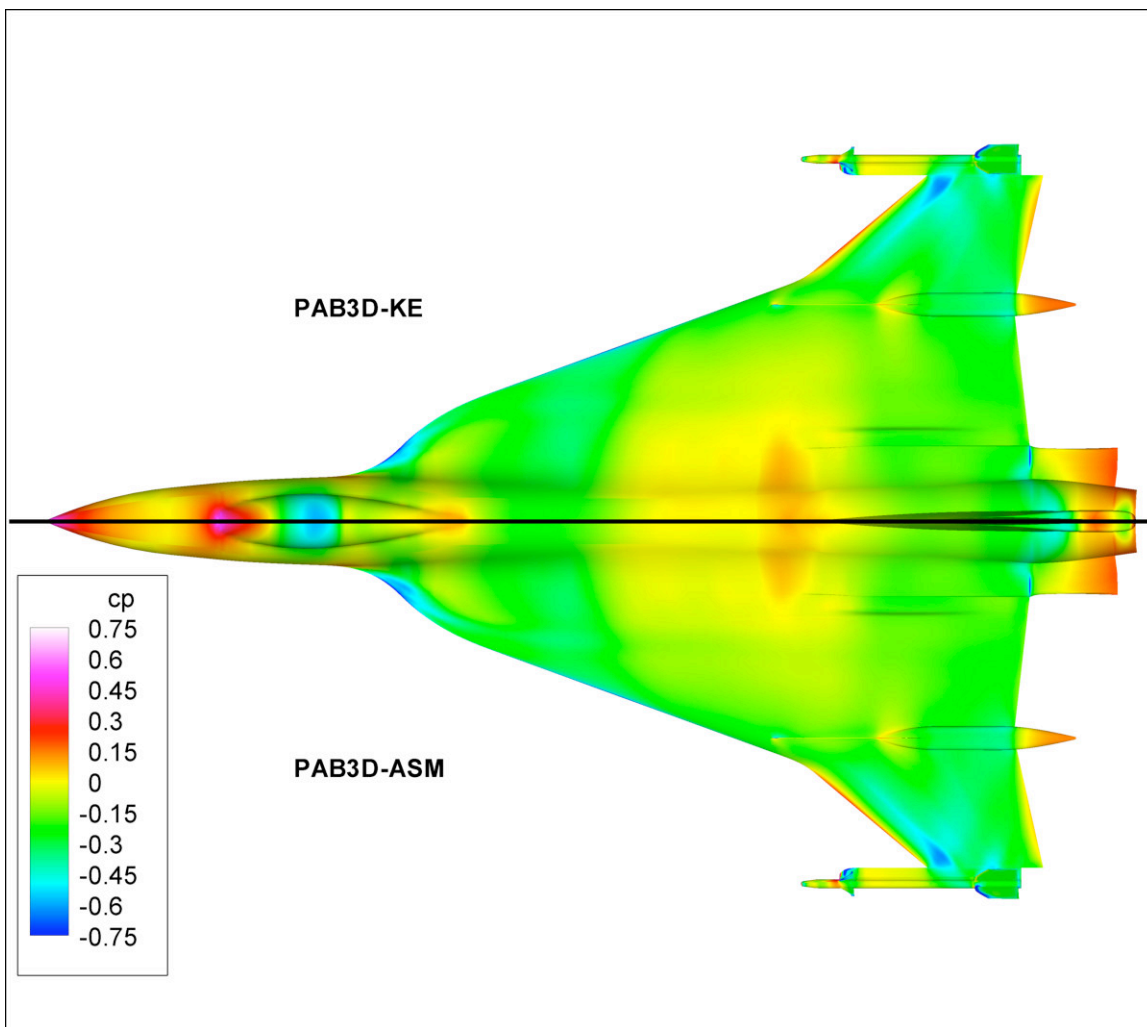
(m) FS 450

(n) FS 492.5

(o) Upper Surface C_p

Figure 15 Concluded